Electronic Supplementary Material (ESI) for Nanoscale.

Supplementary Information

Plasmon-exciton systems with high quantum yield using deterministic aluminium nanostructures with rotational symmetries

Landobasa Y M Tobing[1], Muhammad Danang Birowosuto[2], Kah Ee Fong[1], Yuan Gao[1], Jinchao Tong[1], Fei Suo[1], Cuong Dang[1,2], Hilmi Volkan Demir[1], Dao Hua Zhang[1,*]

*Corresponding author: EDHZHANG@ntu.edu.sg
[1)] School of Electrical and Electronic Engineering, Nanyang Technological University, 50 Nanyang Avenue, 639798, Singapore
[2)] CNRS International NTU Thales Research Alliance (CINTRA), Research Techno Plaza, 50 Nanyang Drive, Border X Block, 637553, Singapore

1. The dynamics of field localizations in gammadion and C_n structures

The dynamics of the E_z and H_z fields were recorded from the movie monitor around the fundamental resonance modes in a commercial finite difference time domain software (*Lumerical* Inc), with the incident input of $E_{inc} = E_x \pm iE_y$ for left circular polarized (LCP) and right circular polarized (RCP) excitations. For the gammadion structure, the dynamics for the E_z and H_z field are respectively given in Movie 1 and Movie 2 (for LCP excitation); and in Movie 3 and Movie 4, respectively (for RCP excitation). Likewise, for the C_n structure, the dynamics for the E_z and H_z field are respectively given in Movie 5 and Movie 6 (for LCP excitation); and in Movie 7 and Movie 8 (for RCP excitation).

2. Characterization of CdSe/CdS colloidal quantum dot

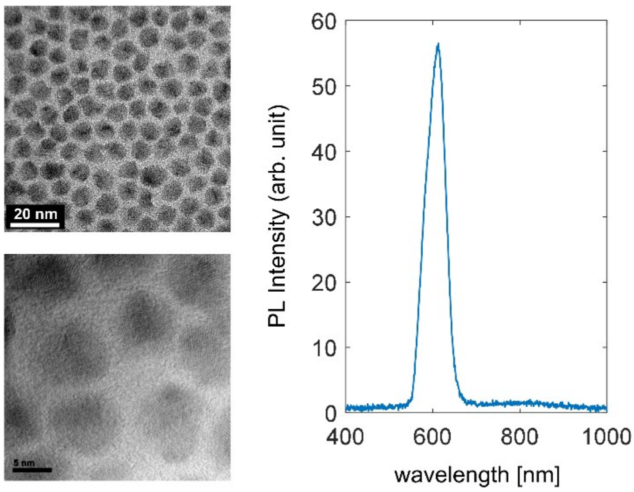

Figure S1. (Left) Transmission electron microscopy (TEM) images of CdSe/CdS quantum dots. (Right) PL measurement of CQD film on quartz substrate $(\lambda_{em} = 615nm, \Delta\lambda_{cqd} = 56nm)$

3. PL intensity mapping of quantum dots in gammadion and star-shaped structures

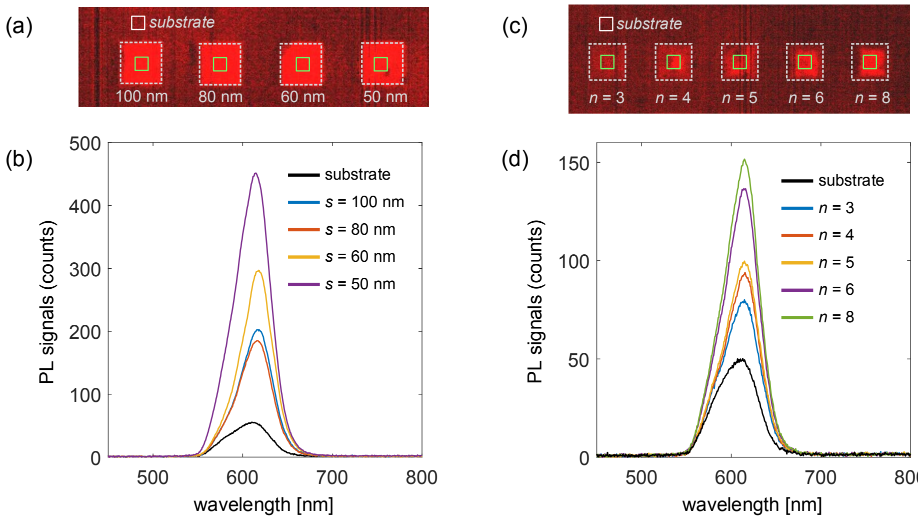

Figure S2. Photoluminescence intensity mapping under 434-nm illumination for the gammadion structures (a) and star-shaped C_n structures (c). The PL intensity signals from the indicated region-of-interest (ROI) for gammadion (b) and star-shaped C_n structures (d). The mapping was performed using 50x objective lens (NA 0.55). The footprint for all the Al nanostructures is 20 microns x 20 microns.

4. Gammadion resonance modes derived from longitudinal and transverse plasmons

The mode analysis of gammadion resonator (me_0 and me_1 modes) from the perspective of superposition of conductively coupled longitudinal plasmons have been studied in detail in our previous work. For Al gammadion resonator, where plasmonic resonance in the UV range can still be supported, there exists additional resonance mode derived from the transverse plasmons. The $|E|$ and E_z field distributions for Al gammadion resonator (with s = 100 nm) are presented in Fig. S2 for X- and Y-polarized excitations. The top and middle rows refer to the resonance modes derived from longitudinal plasmon (me_0 and me_1) and the bottom row refers to the resonance mode derived from transverse plasmon (tme_0). The E_z-field mapping shows the surface charge distributions on the resonator, from which electric dipole representation for each resonance mode can be schematically drawn. Note that the $|E|$-field distribution of the transverse plasmon based tme_0 is qualitatively similar to that of the fundamental me_0 mode, with comparable field enhancement.

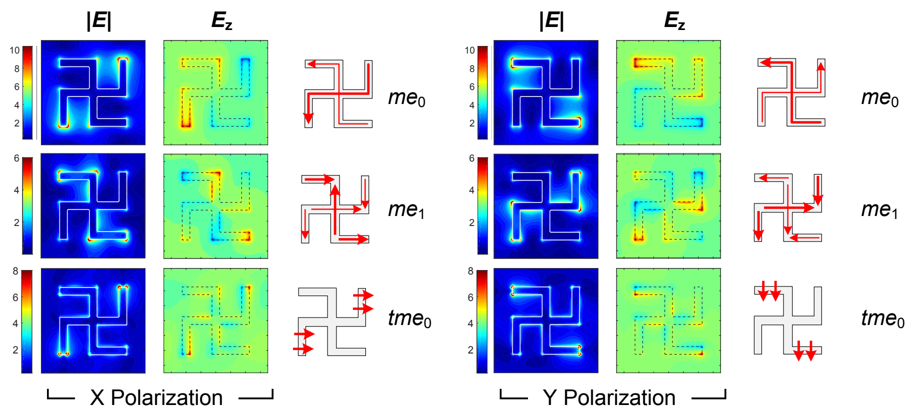

Figure S3. The mode characteristics of gammadion resonance modes. (Top row) the fundamental me_0 mode, (Middle row) higher order me_1 mode, and (Bottom row) transverse plasmon based me_0 mode. The more dominant electric dipoles for each polarization are represented in thicker arrows.

5. Transmission characteristics of gammadion and star-shaped structures

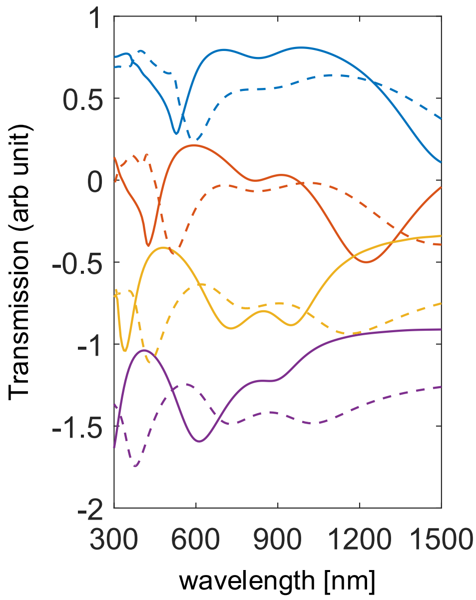

Figure S4. Simulated Al gammadion structures at decreasing side lengths (from s = 100 nm to s = 50 nm) with (dashed) and without (solid) colloidal quantum dot coating. The transmission is vertically offset by 0.6.

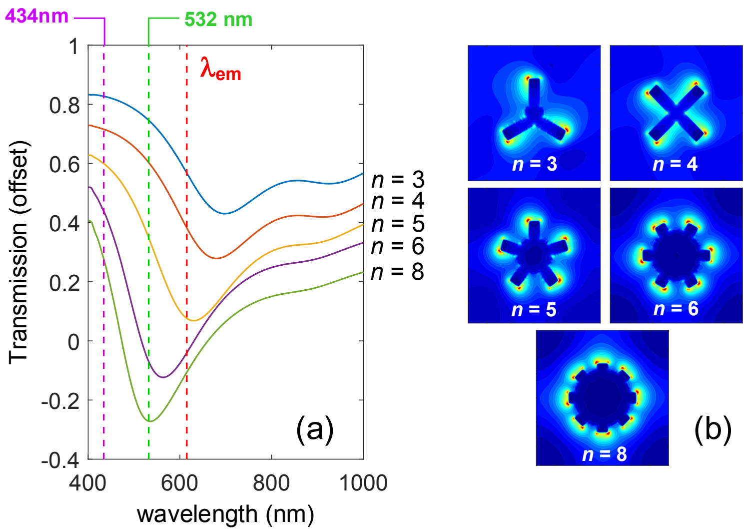

Figure S5. Numerical simulations of C_n structure coated with CdSe/CdS quantum dot film. (a) Transmission characteristics under LCP excitation, (b) Rotationally symmetric $|E|$ field distribution at emission wavelength. The refractive index of the CdSe/CdS quantum dot film is obtained from ellipsometer measurements.

6. Estimation of modified quantum yield in isolated C_6 antenna

Based on the standard deviations in the lifetime distributions (Fig. 5b), the upper and lower bound of the spatially averaged Purcell factors are found to be

$F_{p,meas}^{lower} = (9.13 - 0.45)/(4.86 + 0.39) = 1.65$ and $F_{p,meas}^{upper} = (9.13 + 0.45)/(4.86 - 0.39) = 2.14$. Using calculated filling factor $f = 9.8 \times 10^{-3}$ derived from the mode volume $V_{mod} = 3.53 \times 10^{-4}(\lambda/n)^3$ associated with $|E|^2$ distribution in Fig. 5d, the Purcell factor for a single C_6 antenna is in the range of $68.01 < F_P < 118.25$. Using the relation between quantum yields and Purcell factor, $F_P = (1 - QY)/(1 - QY^{'})$, the range of the modified quantum yield corresponding to a single antenna is found to be $QY^{'} \sim 0.99$ (based on 2 significant digits). A more conservative estimate is based on the assumption that the mode field occupies the areal footprint of the C_6 antenna $(A_{cav} = 4s^2)$, which corresponds to a fill ratio of $f = A_{cav}/p^2 = 0.25$. This gives Purcell factor and modified quantum yield in the range of $3.6 < F_P < 5.56$ and $0.89 < QY^{'} < 0.93$.

The modified quantum yield as a function of Purcell factor (F_P) and quantum yield of the uncoupled quantum dot (QY) can be expressed as $QY^{'}(F_P,QY) = 1 - (1 - QY)/F_P$. The range of QY' resulting from the change in F_P and QY is $\Delta QY^{'} = \Delta F_P(1 - QY)/F_P^2 + \Delta QY/F_P$, showing that the modified quantum yield does not change much when the Purcell factor is very high (>10). Another source of error is in the measurement of the quantum yield of the uncoupled CQD. Based on a typical ±0.05 error in the quantum yield measurements, the modified quantum yield is expected to have additional ±0.01 error in its conservative estimate.

The above estimations, which are based on possible measurement errors, illustrate that the modified quantum yield of CQD coupled to a single antenna is in the near-unity level. In addition to these factors, there is also a possibility of CQD film deterioration over time, which could lead to a decrease in the quantum yield. However, such a longitudinal study for the evolution of quantum yield over time is beyond the scope of this work.